Physica Scripta

PAPER

Interaction of electrons and positrons with two-dimensional artificially generated proton lattice and with carbon lattice

M Al-Ajaleen[1,2] and K Tőkési[1,3]

[1] Institute for Nuclear Research (ATOMKI), Debrecen, 4026, Hungary
[2] University of Debrecen, Doctoral School of Physics, Egyetem tér 1, 4032 Debrecen, Hungary
[3] Centre for Energy Research, Budapest, Hungary

E-mail: tokesi@atomki.hu

Keywords: classical trajectory monte carlo model, many-body collisions, electron scattering, positron scattering

OPEN ACCESS

RECEIVED
17 November 2022

REVISED
7 May 2023

ACCEPTED FOR PUBLICATION
26 May 2023

PUBLISHED
7 June 2023

Abstract

A many-body classical trajectory Monte Carlo (CTMC) method is applied in the study of scattering probabilities of electrons and positrons after interacting with a two-dimensional (2D) artificially generated, uniform lattice, composed of fixed protons. We used different lattice parameters between the protons for different simulations, where the projectiles have kinetic energies of 500 and 1000 eV. We found a very strong focusing of electrons and a very strong defocusing of the positrons at lower lattice parameters. Furthermore, we found, these effects get weaker with increasing lattice parameters. Interesting changes took place at lattice parameters 2 and 3 au. which are close to the lattice parameter between carbon atoms in graphene of value 2.68 au. We also performed a simulation of a defective lattice by removing some protons and noticed distinguishable changes in the spectra compared to the spectra of an ideal lattice. This comparison may open a way for the detection of lattice defects in real samples.

1. Introduction

Two-dimensional (2D) materials are ideally composed of one atomic layer, thus having an ultra-thin thickness. Atoms in the layer may have a different function than internal atoms, and so the increase in the number of surface atoms leads to a change in the morphological features, hence leading to changes in the behaviour of the 2D materials. These materials are unique due to the limited number of atomic layers, their mobility and unprecedented electronic structures and properties that are unparalleled when compared to their bulky counterparts. A 2D lattice shows diverse electrical properties such as a surface state-free nature, high surface area [1], strong light–matter interaction and high optical nonlinearity, which make a 2D material excellent for many emerging applications [2]. The electronic properties of 2D materials lead to an evolution in many fields such as transistors, photonics, biomedical applications, supercapacitors, sensors, and optoelectronics [3–8].

An interaction between a 2d material and projectiles was performed by Labaigt *et al* [9], in which they demonstrated that electron transfer generated by fast ion impact can be employed as a two-dimensional material imaging technique. They used graphene as a target and a keV proton beam as a projectile. Many other studies were performed to investigate the projectile-2D-material interactions to achieve different goals such as altering the morphology of a graphene monolayer [10], investigating the microscopic mechanism of collisions between energetic protons and graphitic carbon nanostructures [11], studying radiation hardness of graphene using proton beam [12].

Following our previous work, when the interaction of electrons and positrons with protons aligned in one-dimension line was investigated [13], in this paper, we present results in collision between electrons and positrons with 2D lattices. At first the lattice is *artificial hypothetical* 2D lattice genarated from protons and in the second case the lattice contain nautral carbon atoms. The dynamic response of the lattice to the projectile is treated in the framework of a classical trajectory Monte Carlo (CTMC) model. The CTMC method is a strong successful theoretical tool used in many-body interaction studies to investigate collision channels such as

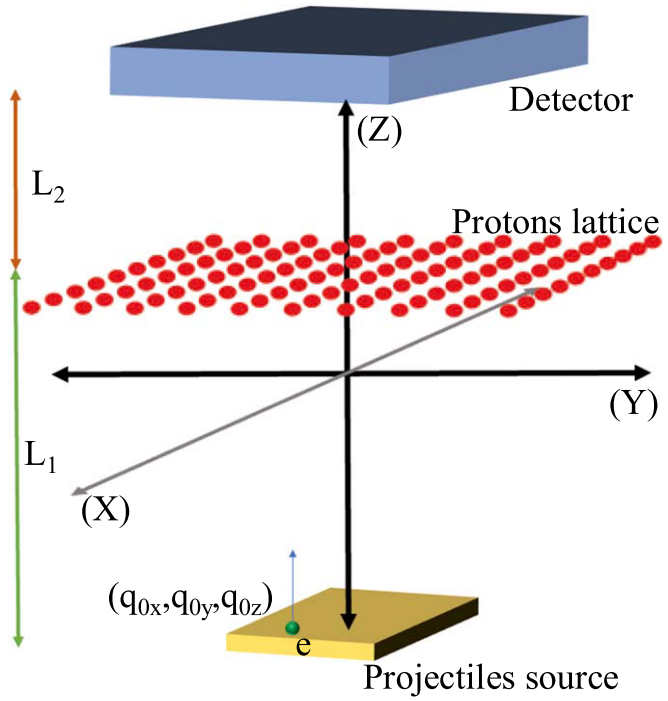

Figure 1. Schematic diagram of the calculation system. L_1 is the distance between the source of the projectiles and the lattice. L_2 is the distance between the lattice and the detector.

ionisation [14–18], excitation [19], electron capture [20, 21] and scattering [22, 23]. In this work, the calculations were performed using two types of targets, an ideal lattice, and a defective lattice in which some protons were removed. The obtained results may open a new way later for the investigation of more realistic targets like graphene. Moreover, the results will show the effectiveness of our imaging scheme in detecting missing protons (vacancies) in the lattice. Atomic units are used throughout the paper unless otherwise indicated.

2. Theory

2.1. The use of the pure coulomb potential

In this work, we used a 10×10 proton lattice, hence, the ionisation, charge transfer and excitation channels do not exist since there are no electrons in the target material. On the other hand, we note, that there is an electron-capture channel for electron impact, but its probability is very weak due to the high kinetic energy of the electron (500 eV and 1 keV), and due to the attractive Coulomb potential in which the electron experiences from the other 99 protons. Hence, based on our model target of a fixed proton lattice, only scattering of the non-destructive electrons and positrons at 500 and 1000 eV energies are studied.

The applied CTMC method is a non-perturbative method, where the classical equations of motions are solved numerically [24]. In the present work, the CTMC simulations were made in the many-body approximation [25, 26], where all protons interact with the projectile. The details of the calculation procedure can be found in [20]. In the present version of the CTMC approach, the protons are fixed, thus in our system, only the projectile has kinetic energy. Coulomb potential is present in the interaction between the projectile and 100 protons. Figure 1 shows the schematic diagram of our system.

The Hamiltonian equation of a projectile and 100 protons lattice can be written as:

$$H = \frac{p^2}{2} + \sum_{i=1}^{100} \frac{Z_0 Z_i}{R_{0i}} \tag{1}$$

where

$$R_{0i} = [(q_{0x} - q_{ix})^2 + (q_{0y} - q_{iy})^2 + (q_{0z} - q_{iz})^2]^{1/2} \tag{2}$$

The equations of motion are given by:

$$\dot{q}_{0k} = p_{0k} \tag{3a}$$

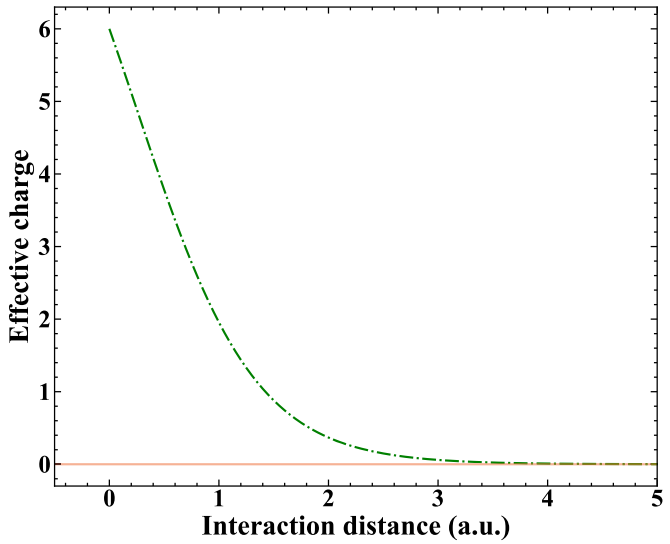

Figure 2. Charge of a carbon atom as a function of intraction distance with the projectiles.

$$\ddot{q}_{0k} = \dot{p}_{0k} = \sum_{i=1}^{100} \frac{Z_0 Z_i (q_{0k} - q_{ik})}{[(q_{0x} - q_{ix})^2 + (q_{0y} - q_{iy})^2 + (q_{0z} - q_{iz})^2]^{3/2}} \tag{3b}$$

where Z_0 and Z_i are the projectile and the proton charge respectively, q is the position vector, and k represents Cartesian coordinates, x, y and z. These equations of motion are solved numerically using the 4th-order Runge–Kutta method for a statistically large number of trajectories for given initial parameters. Regarding position q_0, the projectile has an initial fixed vertical position at $L_1 = 35$ *a.u.* below the lattice, whereas the initial horizontal position is generated randomly (i.e., x and y position). The vertical distance between the detector and the lattice is $L_1 = 40$ *a.u.*

The lattice is uniform and has a constant distance between the protons. During our investigation the lattice parameters are 1, 2, 3 and 5 a.u. The projectile kinetic energies are 500 and 1000 eV, because at lower energies, the projectiles may deflect easily and may avoid the penetration into the lattice. For higher energies than 1000 eV the sum of the Coulomb interaction due to the lattice will have a small effect on the path of the projectiles. Initially, at the beginning of the simulation, the projectiles have non-zero perpendicular velocities, v_z compared to the lattice. The projectile velocities in x and y directions are set to be zero. The source has a geometry $-a \leqslant q_{0x} \leqslant a$ and $-a \leqslant q_{0y} \leqslant b$.

2.2. The use of the pure model potential

In studying the interaction of the projectiles (i.e. electrons and positrons) with a lattice consists of neutral carbon atoms with lattice parameter of 2.72 a.u., we employed a Garvey-type model potential [27] to describe the multi-electronic target system. This model potential is distance dependant, i.e. the charge of the carbon atom depends on the interaction distance with the projectile (see figure 2). Accoring to the figure 2, we can clearly see that the interaction is mostly limited to the distance between 0 au. and 3 au.

The Garvey-type model potentail has the form:

$$V = q\frac{Z - (N-1)(1 - \Omega(r))}{r} \tag{4}$$

where q is a test charge, Z is the atomic number, N is the number of electrons, r is the interaction distance, and $\Omega(r)$ is the screening potential, it has the form:

$$\Omega(r) = [(\eta/\xi)(e^{\xi r} - 1) + 1]^{-1} \tag{5}$$

For small and large interaction distances, the values of $\Omega(r)$ are given by $\lim_{r\to 0}\Omega(r) = 1$ and $\lim_{r\to\infty}\Omega(r) = 0$, respectively. The parameters η and ξ are given by the formulae :

$$\eta = \eta_0 + \eta_1(Z - N) \tag{6a}$$

$$\xi = \xi_0 + \xi_1(Z - N) \tag{6b}$$

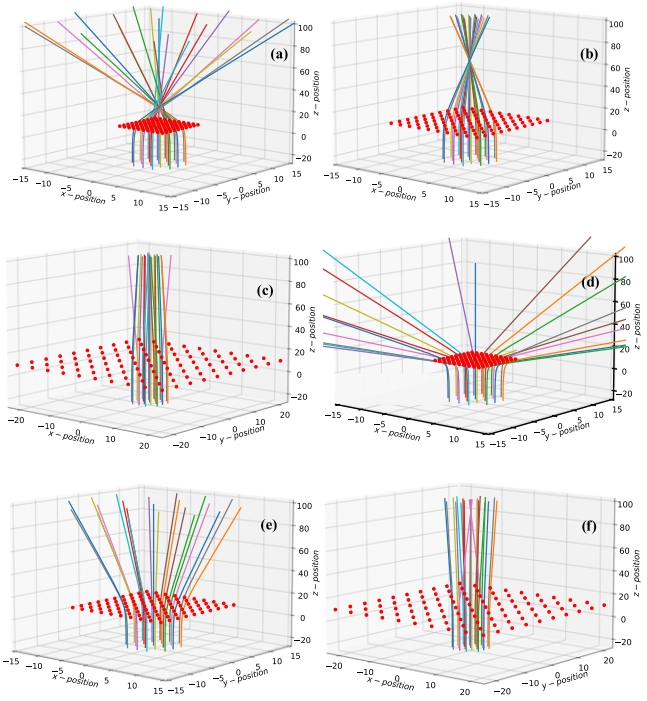

Figure 3. The paths of electrons (panels a, b and c) and positrons (panels d, e and f) passing through the ideal protons lattice. The initial kinetic energies of the projectiles are 1000 eV. The lattice parameters d between two neighbouring protons are (a) 1 a.u., (b) 2 a.u., (c) 5 a.u., (d) 1 a.u., (e) 2 a.u., (f) 5 a.u.

For Carbon, the parameters have the values of $\eta_0 = 2.13$, $\eta_1 = 0.4434$, $\xi_0 = 1.065$ and $\xi_1 = 0.48$ [27]. For more details of the cakculation procedure please see Al-Ajaleen *et al* [28] and the refernces within.

3. Results and discussion

3.1. The case of ideal proton lattice

The paths of the projectiles for electrons and positrons with initial kinetic energy of 1000 eV passing through a proton lattice containing 100 protons in 10×10 configuration are shown in figure 3. For the case of electron projectiles and lattice parameter $d = 1$ *a.u.* we achieved a very strong focusing effect and the focal point is very close to the lattice. Increasing the lattice parameter to $d = 2$ *a.u.* resulted in forming the focal point at a farther distance from the lattice. Increasing the lattice parameter to $d = 5$ *a.u.* leads to form the focal point at a much farther distance from the lattice (see figures 3(a)–(c)). For the case of positron projectiles at lattice parameter $d = 1$ *a.u.*, the deflection of positrons is very high except for those trajectories which are very close to the centre (see figure 2(d)). Increasing the lattice parameter to $d = 2$ *a.u* and $d = 5$ *a.u* resulted in decreasing the trajectory deflection. For the case of $d = 5$ *a.u.*, eventually the paths almost became parallel to each other (see figure 3(f)).

Figure 4 shows the double differential intensity distributions of electrons with kinetic energy of 500 eV after they were scattered from a lattice with $d = 5$ *a.u.* as well as the intensity projection on both x and y axes. We can clearly see that the intensity on x-axis identical to the intensity on y-axis. This is due to the symmetry of the lattice which having the square shape. So, in further discussions it will be sufficient to focus on the x-axis intensity only, except for the case of defective lattice which require the intensities for both axes.

The intensities of electrons and positrons after passing through the 10×10 proton lattice are shown in figure 5. The corresponding double differential intensities are shown in figure 6 and figure 7. The first thing to be noticed is the peculiar peak of 500 eV electrons at lattice parameter $d = 2$ *a.u.* (see figure 5(a)) which have a larger and broader intensity compared to the other lattice parameters. This peculiar peak can be explained according to figures 3(b) and 6(b). The focal point of 500 eV electrons passing through the lattice using lattice parameter $d = 2$ *a.u.* is larger than the focal point using the lattice parameter $d = 1$ *a.u.* (see figures 3(a), and (b)).

From figures 6(a) and (b) we can see the formation of octagram. In case of d = 2 a.u. the octagram is very large compared to the case of $\boldsymbol{d = 1}$ ***a.u.***, and that results the large intensities on the x and y axes projections. Furthermore, at $\boldsymbol{d = 1}$ ***a.u.***, the proton lattice is forcing a large number of the electrons to be focused exactly at

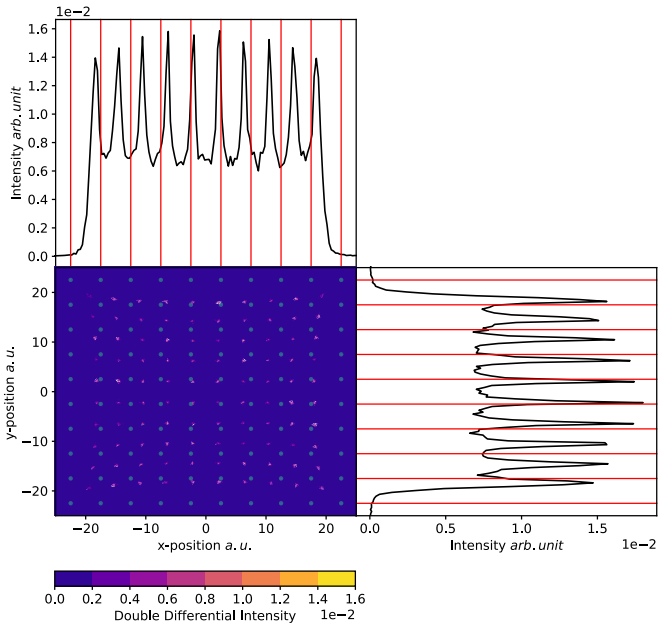

Figure 4. The double differential intensity distributions of electrons at $\boldsymbol{d} = 5\ \boldsymbol{a.u.}$ and at initial kinetic energy of 500 eV. The electron distributions projected in x and y directions are also shown. The green dots and the red lines show the position of the protons.

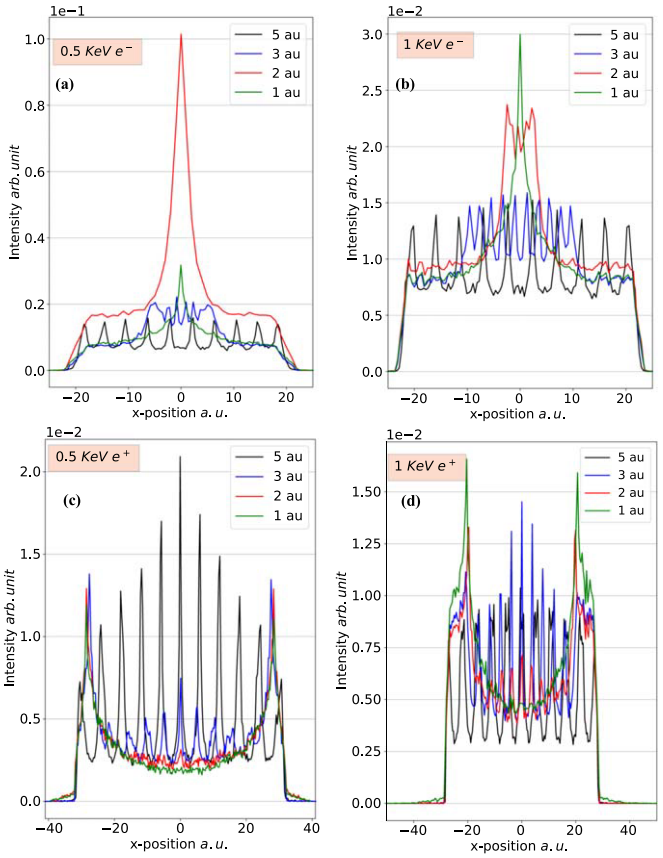

Figure 5. The intensities distributions of electrons and positrons in the projection of x-direction after passing through the 10×10 protons' lattice. The lattice parameters are 1, 2, 3 and 5 a.u. (a) 500 eV electrons, (b) 1000 eV electrons, (c) 500 eV positrons, (d) 1000 eV positrons.

the centre of the detection plane creating a sharp peak. This is due to the high attractive Coulomb force at the edges generated by the centre and other protons. The peak for 1000 eV electrons is slightly broader than that of the 500 eV electrons but both still have almost the same intensities. This is because some of the 1000 eV electrons

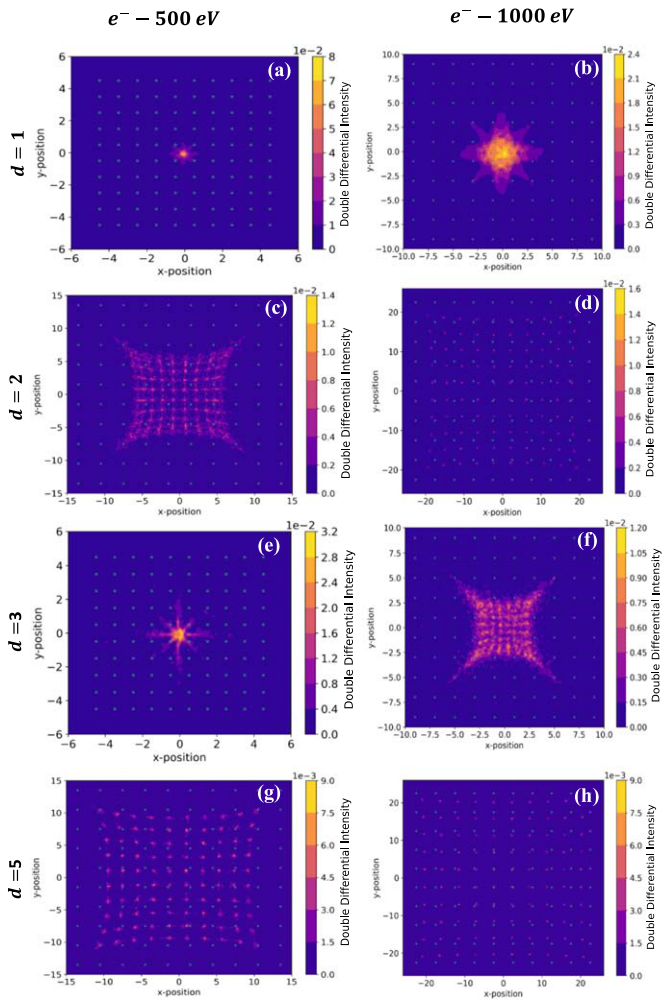

Figure 6. Double differential intensity distributions of electrons after scattering by a 10×10 proton lattice (a)–(d) 500 eV electrons with lattice parameters 1, 2, 3 and 5 a.u., (e)–(h) 1000 eV electrons with lattice parameters 1, 2, 3 and 5 a.u.

have deflected slightly more than the 500 eV electrons around the centre (see figures 5(a), (b) and 6(a), (e)). The electron due to the higher kinetic energy can approach closer the target atoms and thereby may feel stronger Coulomb interactions. Increasing the lattice parameter to $\boldsymbol{d} = 2\ \boldsymbol{a.u.}$ lead to move the focal point farther losing the strong focusing for the 1000 eV electrons. But still most of the electrons are detected close to the centre (see figure 6(b)). From figure 5(b) we can also see that the three peaks are appeared at $\boldsymbol{d} = 2\ \boldsymbol{a.u.}$, two outer sharp edges peak and a smaller inner peak, when increasing the electrons energy from 500 eV to 1000 eV.

Having the lattice parameter larger ($\boldsymbol{d} = 3\ \boldsymbol{a.u.}$) lead to losing the focusing significantly. Furthermore, the electrons show multiple peaks between the protons, especially for the case of electrons at 1000 eV.

It is worth noticing that the case of $\boldsymbol{d} = 3\ \boldsymbol{a.u.}$ with 500 eV electrons is closely similar to the case of $\boldsymbol{d} = 2\ \boldsymbol{a.u.}$ with 1000 eV electrons (see figures 6(c), (f) and (g)). The number of inner peaks are four for 500 eV electrons at $\boldsymbol{d} = 3\ \boldsymbol{a.u.}$ For the 1000 eV electron case, the outer edges became sharper, and the number of inner peaks is eight. The total number of peaks is 10. We can also note that the peaks are more intense compared to the case of 500 eV at the same lattice parameter (see figures 5(a), and (b)). From figure 5(b), we also notice that the intensity dropped when increasing the lattice parameter from 2 to 3 a.u. This is simple because of the electrons at $\boldsymbol{d} = 3\ \boldsymbol{a.u.}$ are distributed on a larger area. Increasing the lattice parameter to $\boldsymbol{d} = 5\ \boldsymbol{a.u.}$, we see that the focusing property is totally lost (i.e., the focal point is at a very large distance from the proton lattice) as shown in figures 6(d) and (h). However, there are minor differences between the 500 eV and 1000 eV cases. Firstly, there is a slight increase in the distance between the peaks for 1000 eV electrons compared to that of the 500 eV electrons. Secondly, the peak intensities for the 500 eV are slightly larger than that of the 1000 eV, but the peaks are smaller. Figures 6(d), and (h) show multiple peaks scattered all over the area of the detector parallel to the position of the protons, which can be understand with the same scenario as for the case of 1000 eV electrons at $\boldsymbol{d} = 3\ \boldsymbol{a.u.}$ (see figure 6(g)).

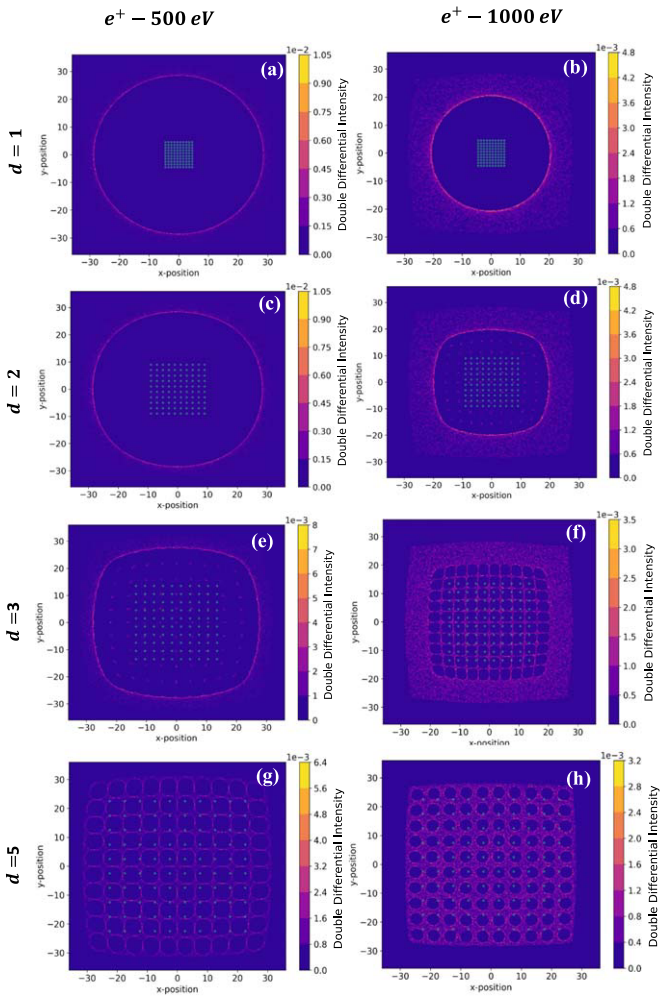

Figure 7. Double differential intensity distributions of positrons after scattering by a 10 × 10 proton lattice (a)–(d) 500 eV positrons with lattice parameters 1, 2, 3 and 5 a.u., (e)–(h) 1000 eV positrons with lattice parameters 1, 2, 3 and 5 a.u.

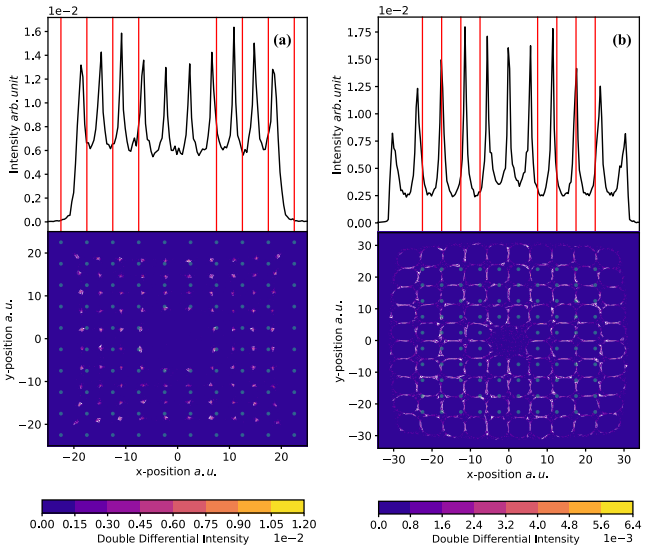

Figure 8. The full intensity distribution of (a) 500 eV electrons (b) positrons and its projection onto the x axis at $\boldsymbol{d} = 5\ \boldsymbol{a.u.}$ The green dots and the red lines show the position of the protons.

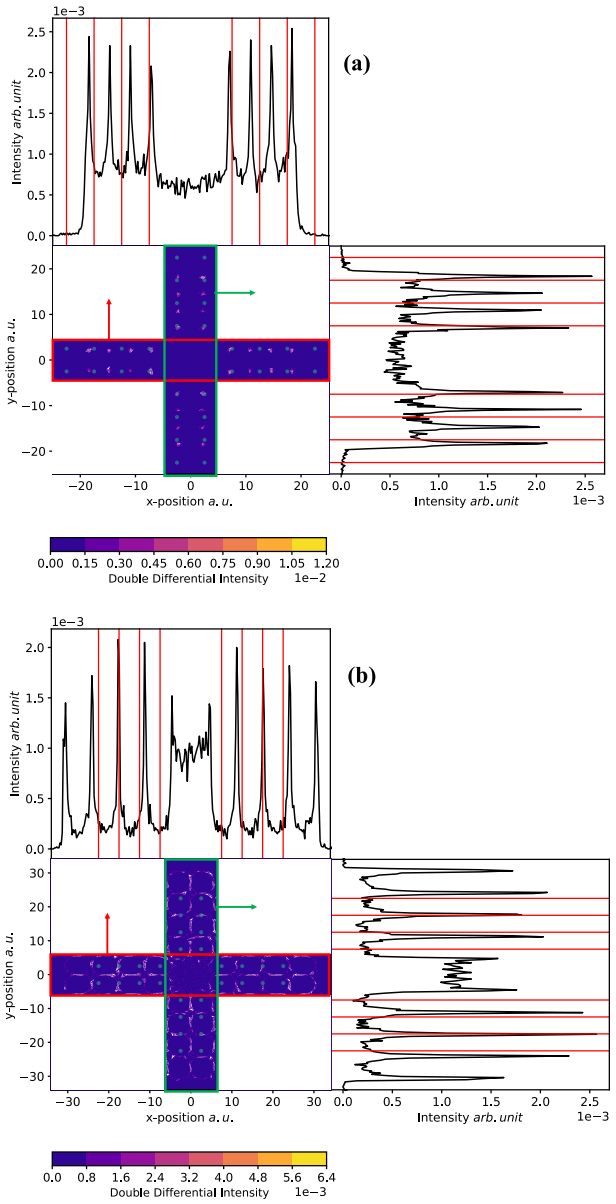

Figure 9. The segment intensity distribution of 500 eV (a) electrons (b) positrons in the x projection and the distance between neighbouring protons $\boldsymbol{d} = 5\ \boldsymbol{a.u.}$. The green dots and the red lines show the position of the protons.

For the case of $\boldsymbol{d} = 1\ \boldsymbol{a.u.}$ at both kinetic energies of 500 eV and 1000 eV, the positrons hit the detector with forming a perfect circle, indicating a clear defocusing which creates anti-cusp due to the high repulsive potential energy. The circle for the case of 500 eV positrons has a radius of almost $14\boldsymbol{a.u.}$, while for the case of 1000 eV positrons has a radius of 10 a.u, (see figures 7(a) and (e)). Moreover, from figures 5(c) and (d), the projection of the intensities on x-axis shows two outer peaks with a valley between them. We found that the intensity of the 1000 eV positrons is higher compared to the case of 500 eV. This can be attributed that at large distance from the lattice the repulsive potential energy is very weak and will have a smaller effect on the higher energy positrons. No significant change in the intensity distributions can be found at 500 eV positron impact and at $\boldsymbol{d} = 1$ and $\boldsymbol{d} = 2$. However, when the kinetic energy is 1000 eV, some of the positrons were able to penetrate between the protons forming small peaks. We can also see that there is a symmetry in the area between the outer peaks, and the middle peak being to be more intense. Moreover, we can also see that the positrons no longer form a circle on the detector. Now they are somehow starting to take the shape of the lattice, which is a square (see figure 7(f)).

For the case of 1000 eV positrons with $\boldsymbol{d} = 3\ \boldsymbol{a.u.}$, we see forming of small cubes on the detector, with the outer cubes being slightly deformed (see figure 7(g)). From figure 5(d) we can also see that the peaks are becoming higher and higher, and starting to surpass the outer peaks. This indicates that most of the positrons can be able to penetrate into the lattice. Increasing the lattice parameter to $\boldsymbol{d} = 5\ \boldsymbol{a.u.}$, leads to changing the

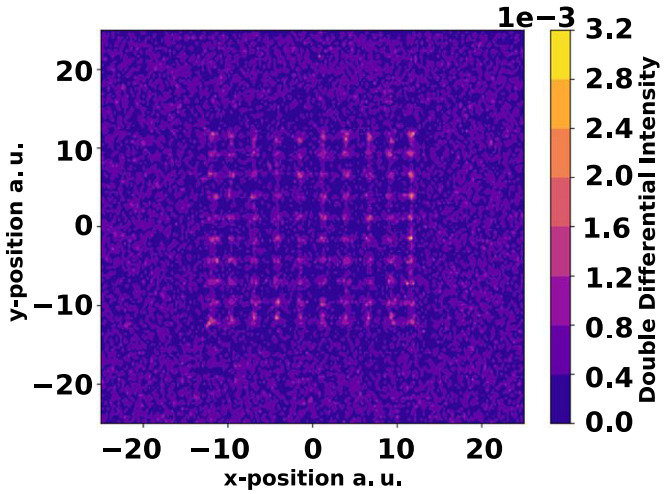

Figure 10. Double differential intensity distributions of electrons passing through a 10 × 10 neutral carbon lattice. The lattice parameter is 2.72 a.u. and the electron initial energy is 1000 eV.

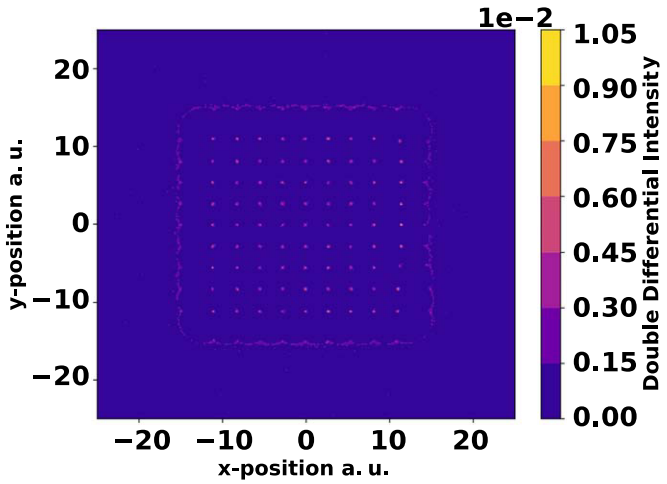

Figure 11. Same as fgure 10, but here the projectiles are positrons.

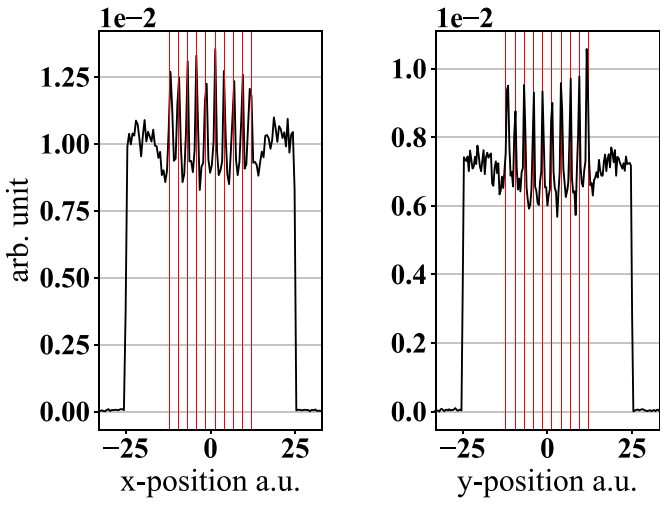

Figure 12. The intensities distributions of electrons in the projection of x- and y-direction after passing through the carbon lattice.

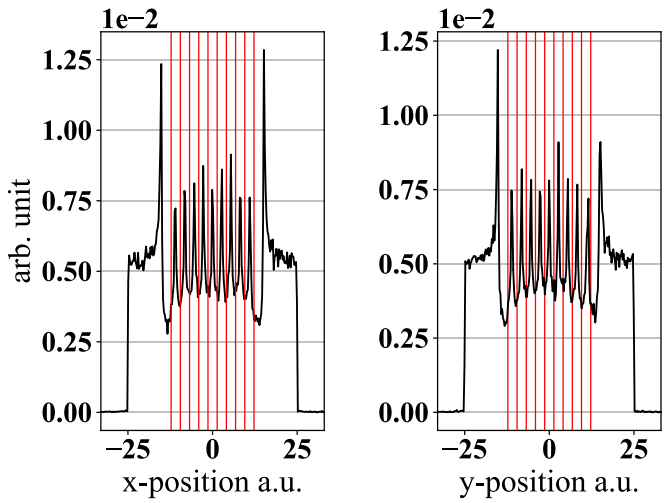

Figure 13. Same as figure 12, but here the projectiles are positrons.

small cubes. In addition, the area between the circles, which is filled with positrons, is thicker in the 1000 eV positrons case compared to the 500 eV (see figures 7(d) and (h)). In the case of 500 eV, the peaks have a symmetrical shape, and they totally surpassed the outer peaks. The middle peaks are now the largest one.

3.2. The case of the defective proton lattice

We repeated our calculation described in our previous section when we removed four protons from the centre of the lattice at d = 5 a.u. to study the changes due to a defective lattice. The coordinates of the removed protons in Cartesian coordinates are (−2.5, −2.5, 10), (−2.5, 2.5, 10), (2.5, −2.5, 10), and (2.5, 2.5, 10). Figure 8 shows the full intensity distribution of electrons and positrons, having kinetic energy of 500 eV, passing through the proton lattice at lattice parameter $\boldsymbol{d} = 5\ \boldsymbol{a.u.}$. Figure 8 shows also the projection of the intensities on the *x*-axis. For both electron and positron cases only slight differences can be obtained in the total intensity distributions in the defected area.

Figures 9(a) and (b) represent a spectrum after probing small segment of the target, the probing focuses on the line in which some protons were removed. For the case of electron impact we found that the peaks vanish in the position of the removed protons. For the case of positron impact, however the peaks are joined together forming a bulky shape with much smaller intensity. According to figures 9(a) and (b), we can identify the location of the position of the defect with a high accuracy by scanning the intensity spectra.

3.3. Neutral carbon lattice

As going closer to the real target sytem, we also performed similar calculations for neutral carbon lattice as we did for . artificially generated proton lattice. Figure 10 shows the double differential intensity distributions of electrons after passing through a 10 × 10 neutral carbon lattice. Figure 11 shows the double differential intensity distributions of positrons after passing through a 10 × 10 neutral carbon lattice. Accordinng to the figures 10 and 11, at first sight, we can conlude that we obtained the similar patters as for the case of artificially generated proton lattice. However, at closer look we also find differences. For the case of electron the spatial spread is more and for the case of positrons the focussing is stronger than that of for the case of proton lattice. However, this is exactly what we can expect because the projectiles feel a charge much greater than one in the interaction period (see figure 2).

Figures 12 and 13 show the intensity distributions of electrons and positrons after passing through the carbon lattice when projected on x- and y- axes. As for the case of double differential intensity distributions, here we also found very similar stuctures as for the case of artificially generated proton lattice. So, in general the calculations with proton lattice may give resonable results for the intensities with much less computation effort than for the case a real target system. We note also, that sure latter we cannot avoide the more detaild and maybe more accurate simulations mimicking the scattering system as close to the reality as possible.

4. Conclusion

We have presented a many-body classical trajectory Monte Carlo modelling for the scattering probabilities of electrons and positrons after interacting with an artificially generated two-dimensional uniform lattice

composed of fixed protons. The used impact energies were 500 eV and 1000 eV. We used different lattice parameters between the protons in our simulations. We found that when the lattice parameter is small ($d = 1$ a.u.) the protons work as a one particle with a big charge, which results in strong focusing for electrons and strong defocusing for positrons. When increasing the lattice parameter between the protons to 3 a.u. or higher we lose the strong focusing effect of the electrons, and defocusing effect for positrons, especially for higher kinetic energy. We also performed a simulation of a defective lattice by removing some protons and noticed distinguishable changes in the spectra compared to the spectra of an ideal lattice. Our work showed that we can detect the position of the defect of the lattice by probing the small segments of the target.

As one step further to the real target system we also performed simulations for target using two-dimensional lattice of carbon atoms. In this case the interaction between the projectiles and the atoms in the lattice were mimic by the Garvey-type model potential. We presented the intensity patterns for both electron and positron projectiles for the case of the carbon lattice. We found that the real carbon lattice behaves like the proton lattice. We found similar intensity patters and intensity distributions as we obtained by the artificially generated proton lattice.

Acknowledgments

This work has been carried out within the framework of the EUROfusion Consortium, funded by the European Union via the Euratom Research and Training Programme (Grant Agreement No 101052200 — EUROfusion). Views and opinions expressed are however those of the author(s) only and do not necessarily reflect those of the European Union or the European Commission. Neither the European Union nor the European Commission can be held responsible for them.

Data availability statement

The data cannot be made publicly available upon publication because no suitable repository exists for hosting data in this field of study. The data that support the findings of this study are available upon reasonable request from the authors.

ORCID iDs

M Al-Ajaleen https://orcid.org/0000-0002-3019-0883
K Tőkési https://orcid.org/0000-0001-8772-8472

References

[1] Cai Z, Liu B, Zou X and Cheng H M 2018 *Chem. Rev.* **118** 6091–133
[2] Yu S, Wu X, Wang Y, Guo X and Tong L 2017 *Adv. Mater.* **29** 1606128
[3] Kumar J, Kuroda M A, Bellus M Z, Han S J and Chiu H Y 2015 *Appl. Phys. Lett.* **106** 123508
[4] Guo Z *et al* 2015 *Adv. Funct. Mater.* **25** 6996–7002
[5] Jakus A E, Secor E B, Rutz A L, Jordan S W, Hersam M C and Shah R N 2015 *ACS Nano* **9** 4636–48
[6] Acerce M, Voiry D and Chhowalla M 2015 *Nat. Nanotechnol.* **10** 313–8
[7] Kou L, Frauenheim T and Chen C 2014 *J. Phys. Chem. Lett.* **5** 2675–81
[8] Zhang Y J *et al* 2018 *2D Mater.* **5** 035002
[9] Labaigt G, Dubois A and Hansen J P 2014 *Phys. Rev.* B **89** 245438
[10] Lehtinen O, Kotakoski J, Krasheninnikov A V and Keinonen J 2011 *Nanotechnology* **22** 175306
[11] Krasheninnikov A V, Miyamoto Y and Tománek D 2007 *Phys. Rev. Lett.* **99** 016104
[12] Mathew S, Chan T, Zhan D, Gopinadhan K, Barman A R, Breese M, Dhar S, Shen Z, Venkatesan T and Thong J T 2011 *Carbon* **49** 1720
[13] Al-Ajaleen M and Tőkési K 2023 *Atoms* **11** 46
[14] Tőkési K, Barna I F and Burgdörfer J 2005 *Nucl. Instrum. Methods Phys. Res. B: Beam Interact. Mater. At.* **233** 307–11
[15] Kavčič M and Tőkési K 2007 *Radiat. Phys. Chem.* **76** 542–5
[16] Ziaeian I and Tőkési K 2020 *Atoms* **8** 27
[17] Atawneh S J A, Asztalos Ö, Szondy B, Pokol G I and Tőkési K 2020 *Atoms* **8** 31
[18] Acebal E and Otranto S 2019 *Eur. Phys. J.* **73** 91 LinkD
[19] Tőkési K 2019 *Nucl. Instrum. Methods Phys. Res. B: Beam Interact. Mater. At.* **233** 266–9
[20] Tőkési K and Hock G 1996 *J. Phys.* B **29** L119–25
[21] Oliveira V, Herbert A, Santos A and Tőkési K 2019 *Eur. Phys. J.* D **73** 146
[22] Tőkési K 2007 *Radiat. Phys. Chem.* **76** 624–6
[23] Sulik B and Tőkési K 2007 *Adv. Quantum Chem.* **52** 253–76
[24] Olson R E and Salop A 1977 *Phys. Rev.* A **16** 531–41
[25] Tőkési K, DuBois R D and Mukoyama T 2014 *Eur. Phys. J.* D **68** 255
[26] Tőkési K and Hock G 1994 *Nucl. Instrum Meth. Phys. Res.* **86** 201–4
[27] Garvey R H, Jackman C H and Green A E S 1975 *Phys. Rev.* A **12** 1144–52
[28] Al-Ajaleen M, Taoutioui A and Tőkési K 2023 *Plasma Phys. Control. Fusion* **65** 065002